~~CONFIDENTIAL~~

Copy
RM H57A02

NACA RM H57A02

RESEARCH MEMORANDUM

NASA TPA #3
2-4-59

STATIC-PRESSURE ERROR CALIBRATIONS FOR NOSE-BOOM AIRSPEED INSTALLATIONS OF 17 AIRPLANES

By Terry J. Larson, Wendell H. Stillwell,
and Katharine H. Armistead

High-Speed Flight Station
Edwards, Calif.

NATIONAL ADVISORY COMMITTEE
FOR AERONAUTICS

WASHINGTON

March 13, 1957

~~CONFIDENTIAL~~

NATIONAL ADVISORY COMMITTEE FOR AERONAUTICS

RESEARCH MEMORANDUM

STATIC-PRESSURE ERROR CALIBRATIONS FOR NOSE-BOOM AIRSPEED INSTALLATIONS OF 17 AIRPLANES

By Terry J. Larson, Wendell H. Stillwell,
and Katharine H. Armistead

SUMMARY

A flight investigation was conducted to determine the static-pressure errors for nose-boom airspeed installations of 17 airplanes. The investigation covered both research-type and service-type aircraft.

The magnitude of static-pressure errors for the airspeed installations of all the airplanes is shown to vary with airplane geometric characteristics which include nose-boom length, fuselage diameter, and nose fineness ratio. The static-pressure errors for airspeed installations of airplanes with neither extremely blunt nor extremely pointed nose shapes correlate well with the ratio of nose-boom length to effective maximum fuselage diameter. The magnitudes of static-pressure errors vary inversely with this ratio and increase considerably as this ratio decreases below about 1.0.

INTRODUCTION

An important phase of the flight-test programs of high-speed aircraft is the determination of the errors involved in the measurement of Mach number. The principal error in determining Mach number, especially at transonic speeds, is the error in the measurement of static pressure because of the pressure field around an aircraft. This error varies for different aircraft configurations and different locations of the static-pressure orifices within the pressure field of a given aircraft.

Although several methods for determining static-pressure errors have been developed and the calibrations for many airplanes have been reported, little information is available on methods for predicting the magnitude of static-pressure error. Since almost all test airplanes and most high-speed military airplanes employ nose-boom pitot-static tubes, it appeared desirable to compare the calibrations of many airplanes having nose-boom

pitot-static tubes to determine whether static-pressure errors can be predicted for similar installations. It was also of interest to determine if the methods of reference 1, for predicting errors ahead of the fuselage nose of two particular bodies of revolution, are applicable to typical high-speed airplane configurations.

As a routine part of the respective flight research programs, static-pressure error calibrations have been made by the NACA High-Speed Flight Station at Edwards, Calif., for 17 aircraft with nose-boom airspeed installations. These calibrations, of which 15 have not been reported previously, are compared to show the effect of Mach number at low angles of attack on static-pressure errors. They are also compared with the methods developed in reference 1 for predicting static-pressure errors. Calibration data of references 2 and 3 are included for completeness and for comparative purposes.

The methods presented should provide a useful means for predicting the position errors of similar airspeed installations.

SYMBOLS

D	effective maximum fuselage diameter, ft
d	effective inlet-duct diameter, ft
l	effective length, ft
M	true Mach number
M'	recorded Mach number
ΔM	Mach number error ($M - M'$)
p	true static pressure, lb/sq ft
p'	recorded static pressure, lb/sq ft
Δp	static pressure error ($p' - p$), lb/sq ft
q_c	true impact pressure, lb/sq ft
q_c'	recorded impact pressure, lb/sq ft
x	distance from nose of airplane to static-pressure orifices, ft
α	angle of attack, deg

INSTRUMENTATION

The three types of pitot-static tubes employed with the test airplanes are presented in figure 1 which shows the shape of the total-pressure tubes and the location of the static-pressure orifices. Type (a) is the standard Kollsman high-speed tube which was used with four of the test airplanes. Type (b), used on three airplanes, differs most from the other two in static-pressure arrangement, having 18 orifices equally spaced around the tube. Type (c) is the standard NACA high-speed pitot-static tube and has been used with 10 of the test airplanes. The static-pressure orifice configurations are similar to type (a), but the arrangement has been modified (ref. 4) to increase the range of insensitivity of the tube to angle of attack. The total-pressure tube is a type relatively insensitive to angle of attack (A-6 of refs. 5 and 6). Listed in table I are the types of pitot-static tubes used with the test airplanes.

Sensitive-type NACA pressure recorders were used to record static and impact pressures.

METHODS

Four basic methods were used to obtain the static-pressure error calibrations: The fly-by method of reference 7, the radar-phototheodolite method of reference 8, the modified radar-phototheodolite method of reference 9, and in one case the pacer method of reference 7.

Airplanes A, B, C, D, H, I, and J were calibrated by the fly-by method at low Mach numbers and the calibrations were extended to higher Mach numbers by the radar-phototheodolite method. Airplanes E, F, G, L, M, N, O, and P were calibrated by the modified radar-phototheodolite method. Airplane Q was calibrated by the pacer method with airplane D used for the reference airplane. Airplane K was calibrated as reported in reference 3.

The conditions under which the airplanes were calibrated varied considerably since calibration data were seldom obtained during data runs made exclusively for static-pressure error calibration. For example, calibration data for airplane P were obtained at altitudes from 5,000 feet to 30,000 feet, whereas data for airplane O were obtained at altitudes from 30,000 feet to 60,000 feet. These airplanes were calibrated by the same basic method, but the actual calibration procedures depended largely on the respective flight programs.

ACCURACIES

Accuracies of the static-pressure error calibrations vary with method, altitude and Mach number, and type of pitot-static tube. The fly-by method, used at subsonic speeds, is considered the most accurate method. Therefore, data for the airplanes calibrated by this method are more accurate than data obtained by either of the other three methods. The accuracy of calibration data obtained by the modified radar-phototheodolite method shows considerable variations over the altitude range, and large differences in accuracies of various calibrations made by this method are evidenced.

The inherent errors of the pitot-static tubes alone must be considered. References 4, 10, and 11 have shown that the errors of tubes of types (a) and (b) are small. Unpublished wind-tunnel tests of a tube similar to type (c) show that the error is also small for a tube of this type. Therefore, the effect of the different tubes is believed to be small in comparison with the static-pressure errors caused by an airplane, and no attempts are made to compare the static-pressure errors of the tubes.

The errors of the pitot-static tubes caused by the effects of angle of attack and angle of sideslip depend largely on the orifice arrangement of the tubes. References 2 to 4 and 10 and 11 have shown that for tubes of types (a) and (b) these effects are small at low angles of attack and sideslip. The effects of angle of attack on errors for pitot-static tubes of type (c) are shown in figure 2 for airplane N at a Mach number of 0.80. It is seen that the error caused by angle-of-attack effects is insignificant at angles of attack below about 12°. Since the calibration data for all the airplanes were selected for flight conditions at low angles of attack and sideslip, the errors contained in the calibrations from flow angularity effects are considered negligible.

Although it is difficult to specify the exact accuracy of each calibration, the overall accuracy for Mach numbers at low subsonic speeds and supersonic speeds is within ± 0.010, and for Mach numbers at transonic speeds is within ± 0.020.

RESULTS AND DISCUSSION

Presentation of Static-Pressure Error Calibrations

Presented in figures 3 to 16 are the static-pressure error calibrations for nose-boom airspeed installations of 17 airplanes. Included with each figure is a two-view drawing of the particular test airplane.

Calibration data extend from a Mach number of 0.24 for airplane I to a Mach number of 1.50 for airplane M. For the calibration flights, tests on some airplanes were restricted to a specified Mach number range, therefore the data do not necessarily show the performance limits of the airplanes. The curves showing ΔM and $\Delta p/q_c'$ as functions of Mach number were computed from the faired curves showing the data points for M' as a function of M.

Shown in figure 4 is the calibration from reference 2 for airplane B. Figure 5 shows the calibration for airplane C, a later version of airplane B having the same configuration but a nose boom of different type and length.

For airplane D the wing sweep angle may be varied from 20° to 59° in flight. Although most of the calibration data were obtained with the wing in the 59°-sweep position, no measurable differences were noted in the static-pressure errors at other sweep angles.

Figure 11 shows the calibrations for airspeed installations of airplanes I and J. The nose-boom installations are identical; the only differences in the airplanes are the larger wing-tip tanks and a slightly longer nose for airplane J. The calibrations show good agreement, indicating that the small differences between the airplanes do not appreciably affect the static-pressure errors.

The calibration for airplane K (fig. 12) has been reported previously in reference 3. The symbol points of figure 12 represent the calibration for airplane L. These two airplanes, having the shortest booms (2.75 ft) of the test airplanes, differ only in wing and tail thickness and have similar nose-boom installations. The calibrations show excellent agreement.

Airplanes N and O have identical configurations except for the jet engine inlets located well back along the fuselage of airplane N. Since airplane O is rocket powered, it does not have inlets. The nose-boom installations of the two airplanes are identical. From the good agreement shown for these calibrations (fig. 14) and the calibrations for airplanes I and J (fig. 11) and K and L (fig. 12), it appears the same calibrations can be applied to similar airplanes with identical nose-boom airspeed installations.

Airplane Q (fig. 16) is a large bomber-type with the longest nose boom (10.17 ft) of the test airplanes.

Comparison of Static-Pressure Error Calibrations

A comparison of the ΔM curves of figures 3 to 16 shows that the general shapes of these curves are fairly consistent; at subsonic speeds

the Mach number errors increase linearly, at transonic speeds the errors increase rapidly, and at low supersonic speeds the errors drop to zero or near zero. Although the static-pressure error is expected to be zero after the bow shock wave passes the static-pressure orifices, a small error is shown for some airplanes. The maximum Mach number error varies from 0.05 at a Mach number of 1.015 for airplane P to 0.14 at a Mach number of 1.060 for airplanes K and L.

Method using x/D.- Shown in table I are nose-boom and airplane dimensions and the ratio x/D for the test airplanes. The nose-boom length x was determined as the distance from the nose of the airplane to the static-pressure orifices. For the pointed-nose airplanes the measurement is made from the projected end of the nose without the nose boom installed. The effective maximum fuselage diameter is defined as the diameter of a circle having the same area as the maximum fuselage cross section including the area of any duct.

Presented in figure 17 is the variation of Mach number errors with x/D for the various airplanes. Good correlation is shown in the Mach number range of 0.60 to 0.80 for all the airplanes except airplane P. The agreement is not as good in the Mach number range from 0.90 to 1.02, with the poorest correlation shown by airplanes D and P. It is of interest to note that airplanes D and P represent extremes of the nose configurations, having the most blunt and most pointed nose shapes, respectively. Although the agreement is not exact for all airplanes, it appears that reasonable correlation of static-pressure errors throughout the Mach number range is obtained. These data show that static-pressure errors vary inversely with the ratio of the nose-boom length to the effective maximum fuselage diameter. It is seen that this ratio becomes more critical in affecting static-pressure errors for x/D values less than about 1.0.

Method using $(l/D)^2$ and x/l.- Another method for relating static-pressure errors is presented in reference 1. This method, which takes into account the fineness ratio of the fuselage, might be expected to eliminate the discrepancies noted for the comparison based on x/D. The method of reference 1 was developed from a comprehensive investigation of errors ahead of pointed-nose parabolic-arc bodies of revolution having identical thickness distributions; therefore, it is of interest to test the method with typical high-speed airplanes which have widely varying thickness distributions and which cannot be considered true bodies of revolution.

In reference 1, the static-pressure error multiplied by the square of the effective fineness ratio $\Delta p/q_c(l/D)^2$ was shown to be dependent on the ratio of distance ahead of the nose to the effective fuselage length x/l. This comparison was made for speeds below body critical Mach number and for speeds corresponding to the peak static-pressure

error (static-pressure error immediately prior to the passage of bow shock wave). Above body critical Mach number, $\Delta p/q_c(l/D)^2$ is compared with $(l/D)^2(M - 1)$ for various values of x/l.

The data for the present test airplanes were compared by these methods and showed good agreement below body critical Mach number and at peak static-pressure error. Between the critical Mach number and the Mach number for peak static-pressure error, the comparison based on $(l/D)^2(M - 1)$ showed poor agreement.

Because of good agreement of the data for all airplanes based on x/l, at speeds below body critical Mach number and at speeds corresponding to the peak static-pressure error, a comparison on this basis was made over the entire Mach number range. The results of this comparison are shown in figure 18 for the variation of $(l/D)^2\Delta M$ with x/l. To make a more direct comparison with figure 17, ΔM has been substituted for $\Delta p/q_c$ in figure 18, the two quantities being interchangeable at any given Mach number. The quantities d, l, x/d, x/l, and l/D for the test airplanes of this investigation are shown in table I. The effective fuselage length l is defined as twice the distance from the nose to the maximum fuselage diameter. The good agreement over the Mach number range is evident; the two airplanes (D and P) which showed the poorest correlation with the other airplanes when based on x/D correlated well in figure 18. It appears that static-pressure errors for airplanes with practically any type of fuselage nose shape can be related on the basis of $\Delta M(l/D)^2$ and x/l. However, figure 17 indicates that for airplanes with neither extremely pointed nor extremely blunt fuselage nose shapes static-pressure errors can be related to the simple parameter x/D.

Method using x/d.- Reference 1 also presents data for static-pressure errors ahead of open-nose air-inlet bodies of revolution. Static-pressure error was shown to be dependent on the ratio of distance ahead of the inlet to inlet diameter x/d. The variation of static-pressure error with x/d for the six test airplanes with nose inlets is shown in figure 19. The correlation is not as good as that shown in figure 17 for the comparison based on x/D. It appears that the method of reference 1 for determining static-pressure error ahead of nose inlet does not apply to static-pressure error ahead of typical airplane nose-inlet configurations.

CONCLUDING REMARKS

Measurement of the static-pressure errors of 17 nose-boom airspeed installations indicates that: The magnitude of static-pressure errors

for the airspeed installations of all the airplanes is shown to vary with airplane geometric characteristics which include nose-boom length, fuselage diameter, and nose fineness ratio. The static-pressure errors for airspeed installations of airplanes with neither extremely blunt nor extremely pointed nose shapes correlate well with the ratio of nose-boom length to effective maximum fuselage diameter. The magnitudes of static-pressure errors vary inversely with this ratio and increase considerably as this ratio decreases below about 1.0.

High-Speed Flight Station,
National Advisory Committee for Aeronautics,
Edwards, Calif., December 12, 1956.

REFERENCES

1. O'Bryan, Thomas C., Danforth, Edward C. B., and Johnston, J. Ford: Error in Airspeed Measurement Due to the Static-Pressure Field Ahead of an Airplane at Transonic Speeds. NACA Rep. 1239, 1955.

2. Thompson, Jim Rogers, Bray, Richard S., and Cooper, George E.: Flight Calibration of Four Airspeed Systems on a Swept-Wing Airplane at Mach Numbers Up to 1.04 by the NACA Radar-Phototheodolite Method. NACA TN 3526, 1955. (Supersedes NACA RM A50H24.)

3. Goodman, Harold R., and Yancey, Roxanah B.: The Static-Pressure Error of Wing and Fuselage Airspeed Installations of the X-1 Airplanes in Transonic Flight. NACA RM L9G22, 1949.

4. Gracey, William, and Scheithauer, Elwood F.: Flight Investigation at Large Angles of Attack of the Static-Pressure Errors of a Service Pitot-Static Tube Having a Modified Orifice Configuration. NACA TN 3159, 1954.

5. Gracey, William, Coletti, Donald E., and Russell, Walter R.: Wind-Tunnel Investigation of a Number of Total-Pressure Tubes at High Angles of Attack - Supersonic Speeds. NACA TN 2261, 1951.

6. Gracey, William, Letko, William, and Russell, Walter R.: Wind-Tunnel Investigation of a Number of Total-Pressure Tubes at High Angles of Attack - Subsonic Speeds. NACA TN 2331, 1951. (Supersedes NACA RM L50G19.)

7. Huston, Wilber B.: Accuracy of Airspeed Measurements and Flight Calibration Procedures. NACA Rep. 919, 1948. (Supersedes NACA TN 1605.)

8. Zalovcik, John A.: A Radar Method of Calibrating Airspeed Installations on Airplanes in Maneuvers at High Altitudes and at Transonic and Supersonic Speeds. NACA Rep. 985, 1950. (Supersedes NACA TN 1979.)

9. Brunn, Cyril D., and Stillwell, Wendell H.: Mach Number Measurements and Calibrations During Flight at High Speeds and at High Altitudes Including Data for the D-558-II Research Airplane. NACA RM H55J18, 1956.

10. Stivers, Louis S., Jr., and Adams, Charles N., Jr.: High-Speed Wind-Tunnel Investigation of the Effects of Compressibility on a Pitot-Static Tube. NACA RM A7F12, 1947.

11. Hensley, Reece V.: Calibrations of Pitot-Static Tubes at High Speeds. NACA WR L-396. (Formerly NACA ACR, July 1942.)

TABLE I.- GEOMETRIC CHARACTERISTICS OF THE TEST AIRPLANES

Airplane	Type of pitot-static tube	x, ft	D, ft	d, ft	l, ft	x/D	x/d	x/l	l/D
A	b	5.34	4.14	1.65	16.0	1.29	3.24	0.33	3.86
B	a	10.0	5.5	1.74	18.0	1.82	5.75	.56	3.27
C	c	6.7	5.5	1.74	18.0	1.22	3.85	.37	3.27
D	c	5.77	5.25	1.65	20.2	1.10	3.50	.29	3.85
E	c	6.0	5.83	2.39	27.3	1.03	2.51	.22	4.68
F	c	4.71	5.53	1.67	25.4	.85	2.82	.18	4.59
G	c	6.85	6.16	----	36.6	1.11	----	.19	5.94
H	b	3.24	4.29	----	12.6	.76	----	.26	2.94
I	a	8.62	7.2	----	36.2	1.2	----	.24	5.03
J	a	8.62	7.2	----	36.7	1.2	----	.23	5.10
K	a	2.75	4.6	----	21.0	.6	----	.13	4.56
L	b	2.75	4.6	----	21.0	.6	----	.13	4.56
M	c	3.19	4.7	----	19.2	.68	----	.17	4.08
N	c	4.75	5.0	----	24.4	.95	----	.19	4.88
O	c	4.75	5.0	----	24.4	.95	----	.19	4.88
P	c	5.7	5.94	----	80.0	.96	----	.07	13.50
Q	c	10.17	13.1	----	40.6	.78	----	.25	3.10

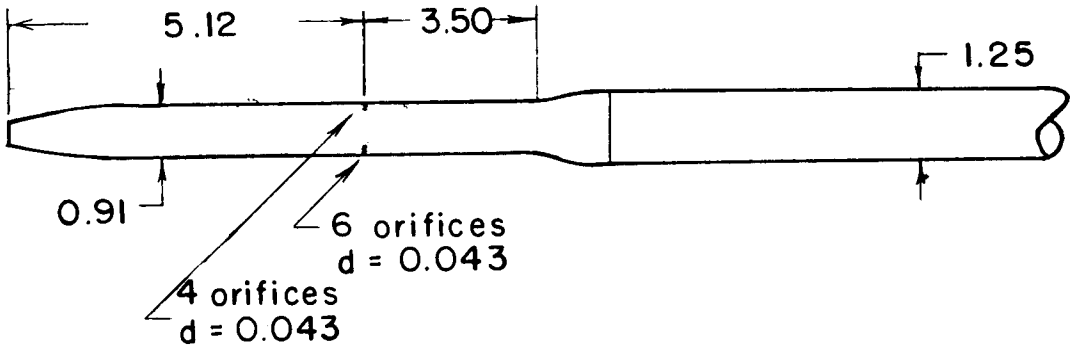

(a) Kollsman high-speed pitot-static tube (ref. 3).

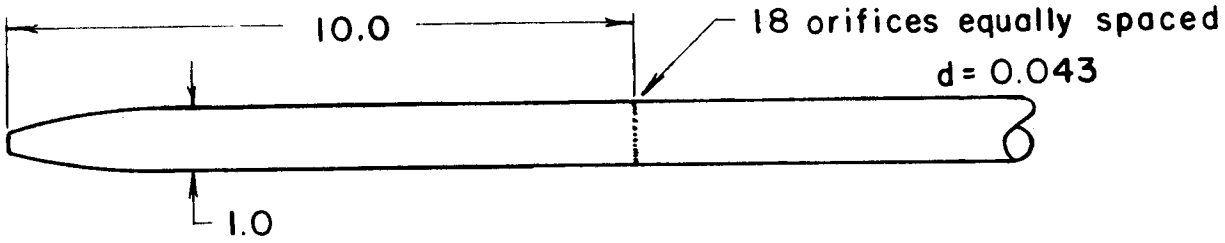

(b) NACA pitot-static tube (ref. 3).

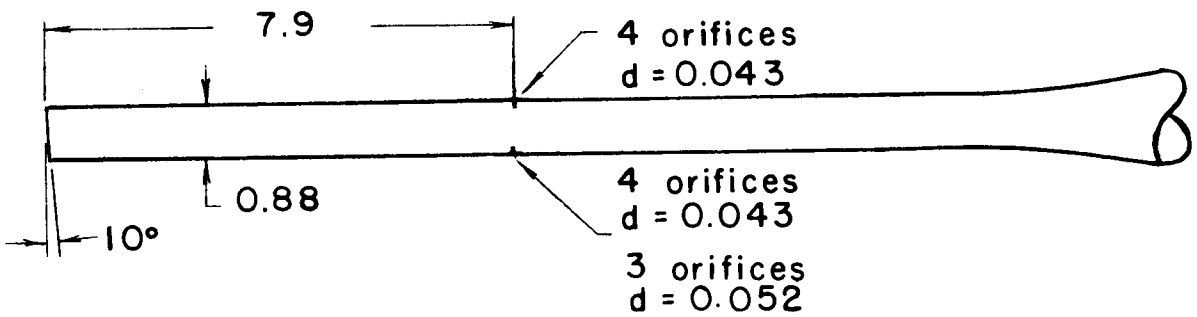

(c) NACA high-speed pitot-static tube (ref. 9).

Figure 1.- Drawings of airspeed tubes used on test airplanes. All dimensions in inches.

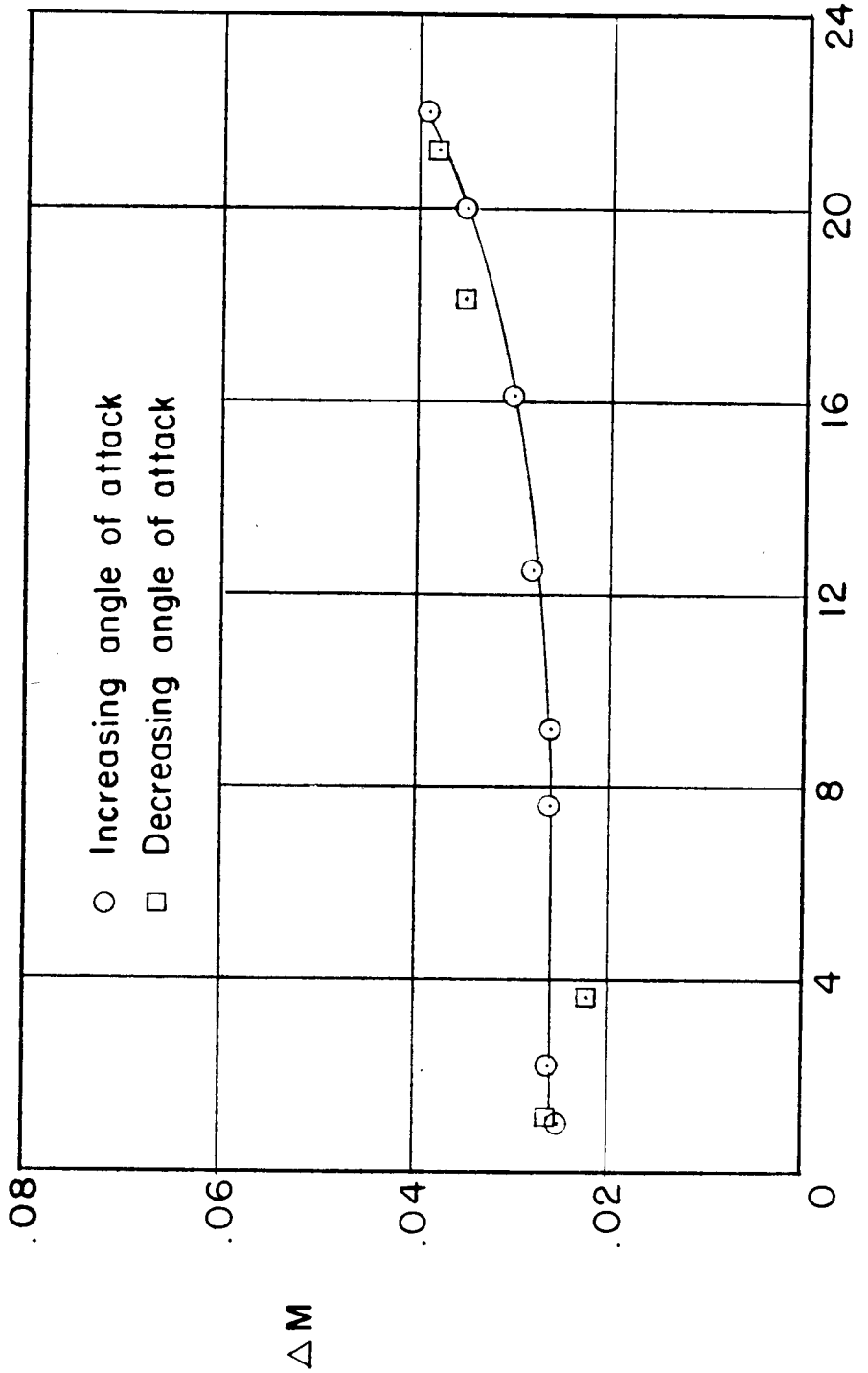

Figure 2.- Variation of static-pressure error with angle of attack for airplane N. M = 0.80.

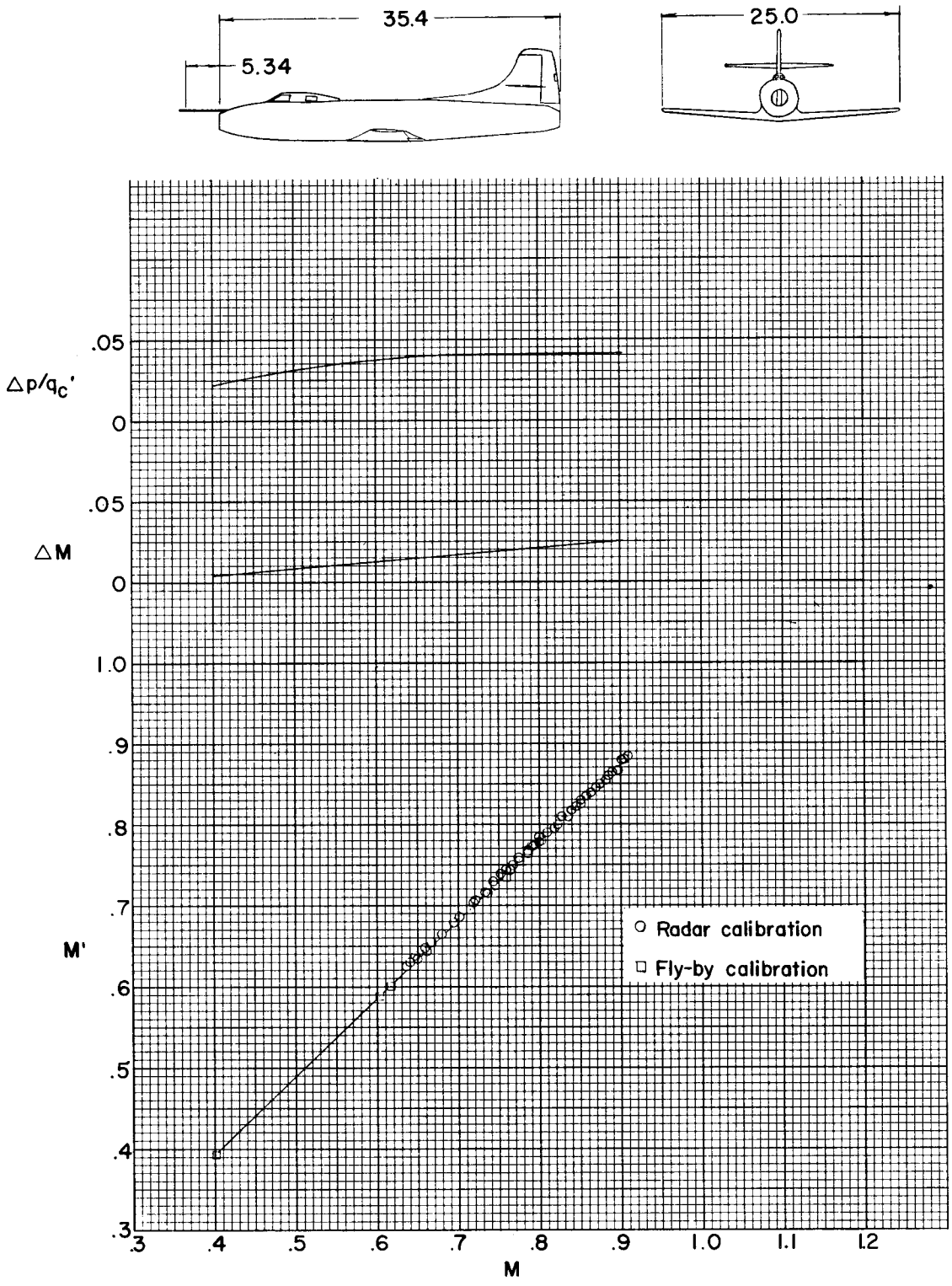

Figure 3.- Static-pressure errors for airplane A.

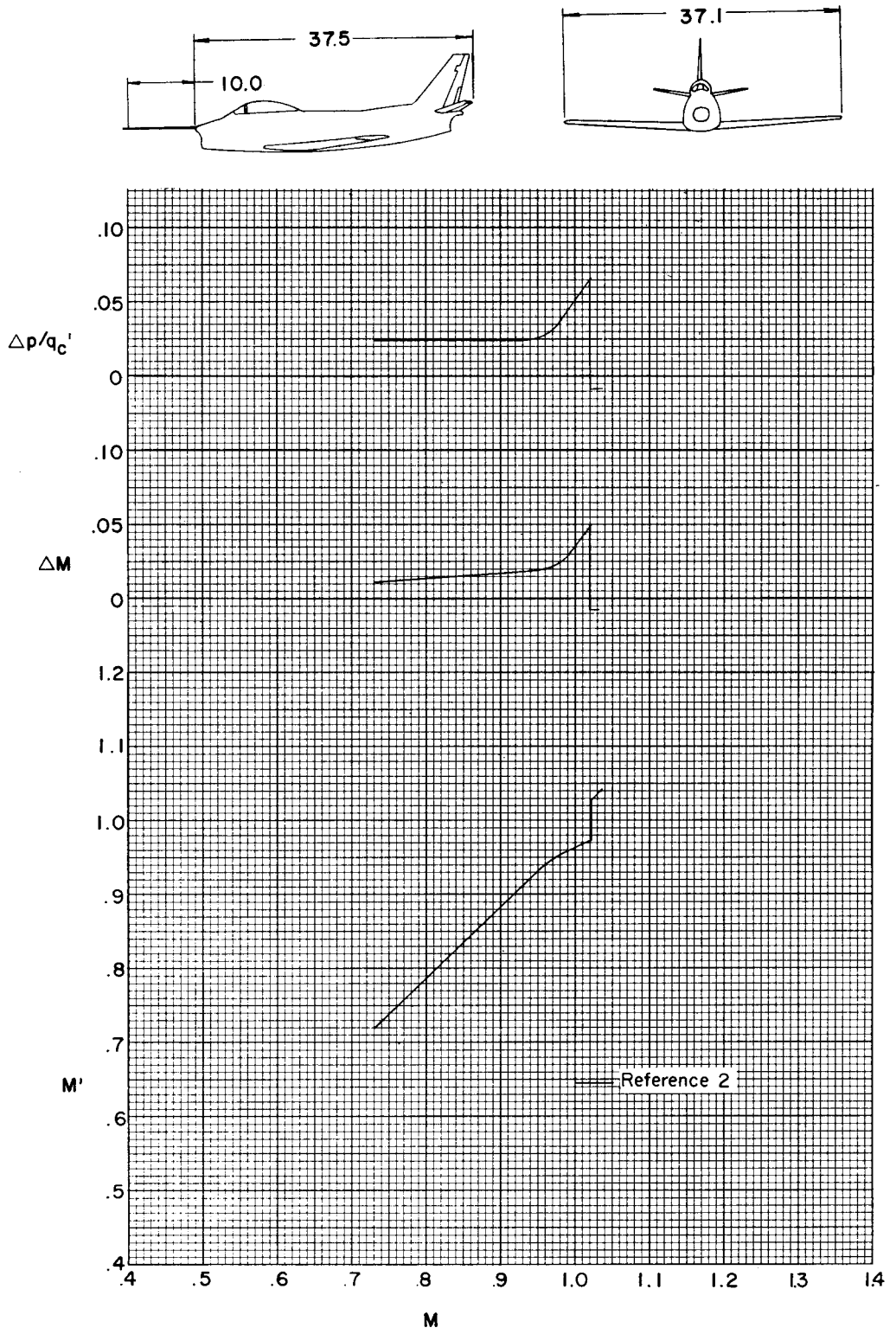

Figure 4.- Static-pressure errors for airplane B.

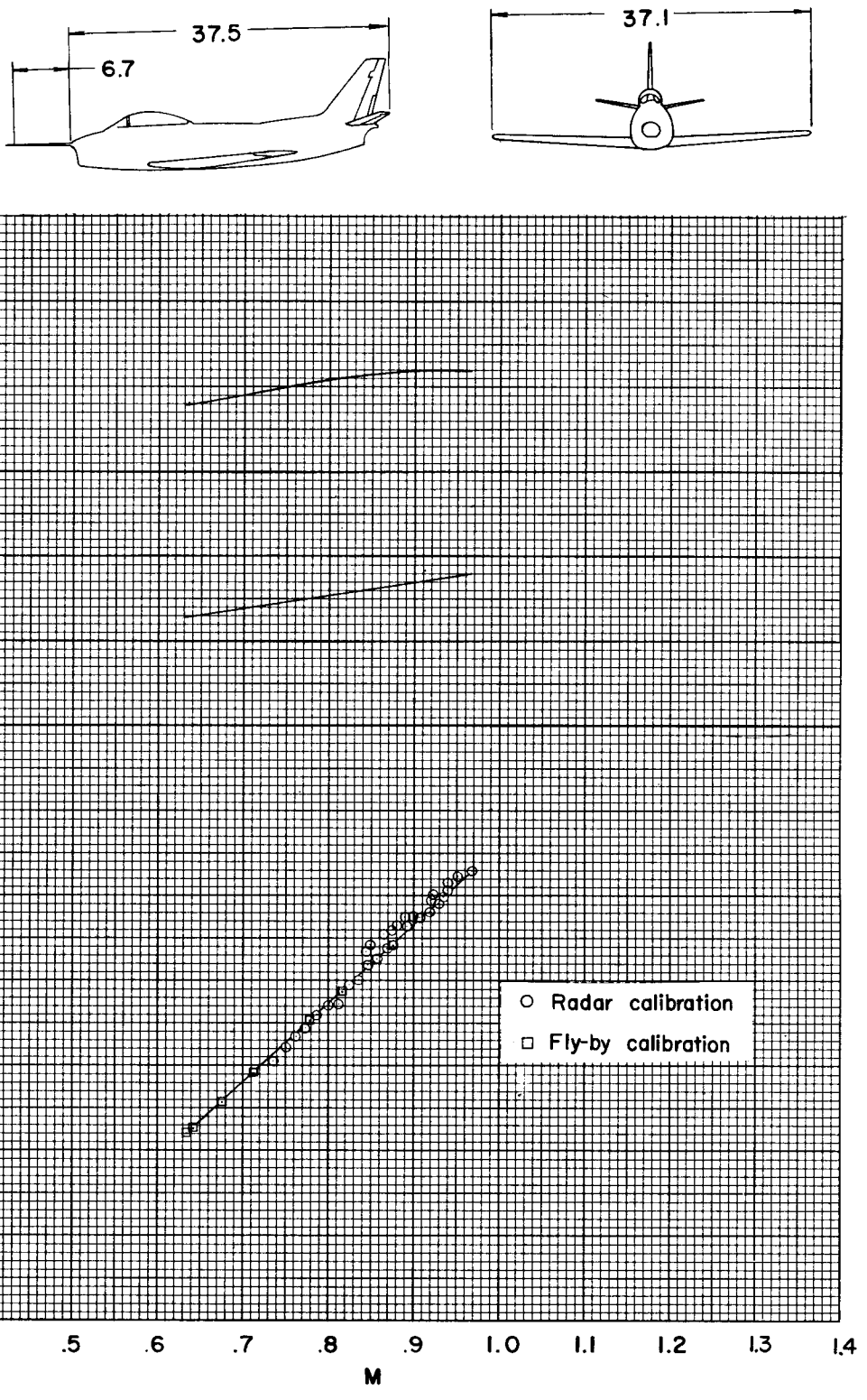

Figure 5.- Static-pressure errors for airplane C.

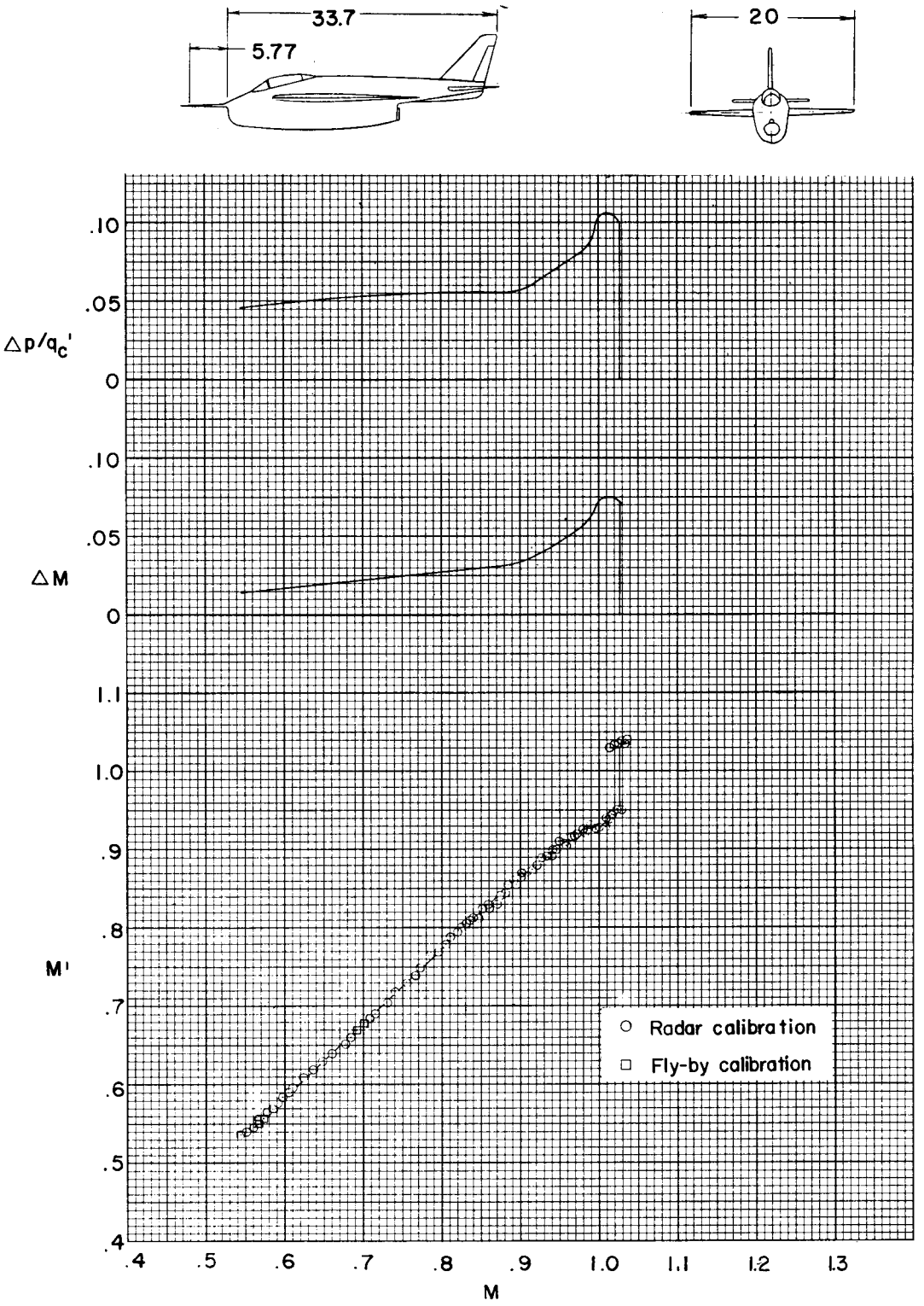

Figure 6.- Static-pressure errors for airplane D.

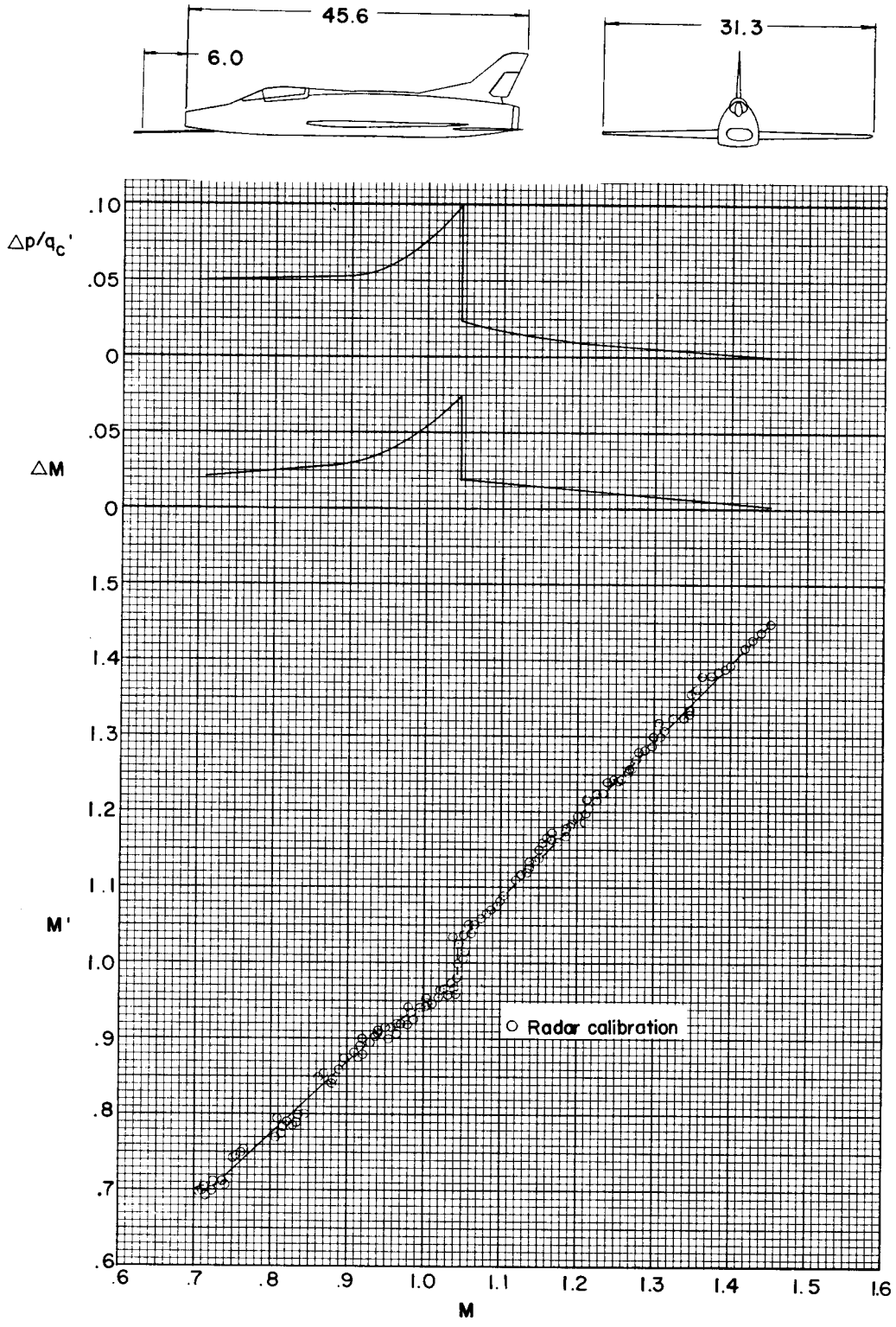

Figure 7.- Static-pressure errors for airplane E.

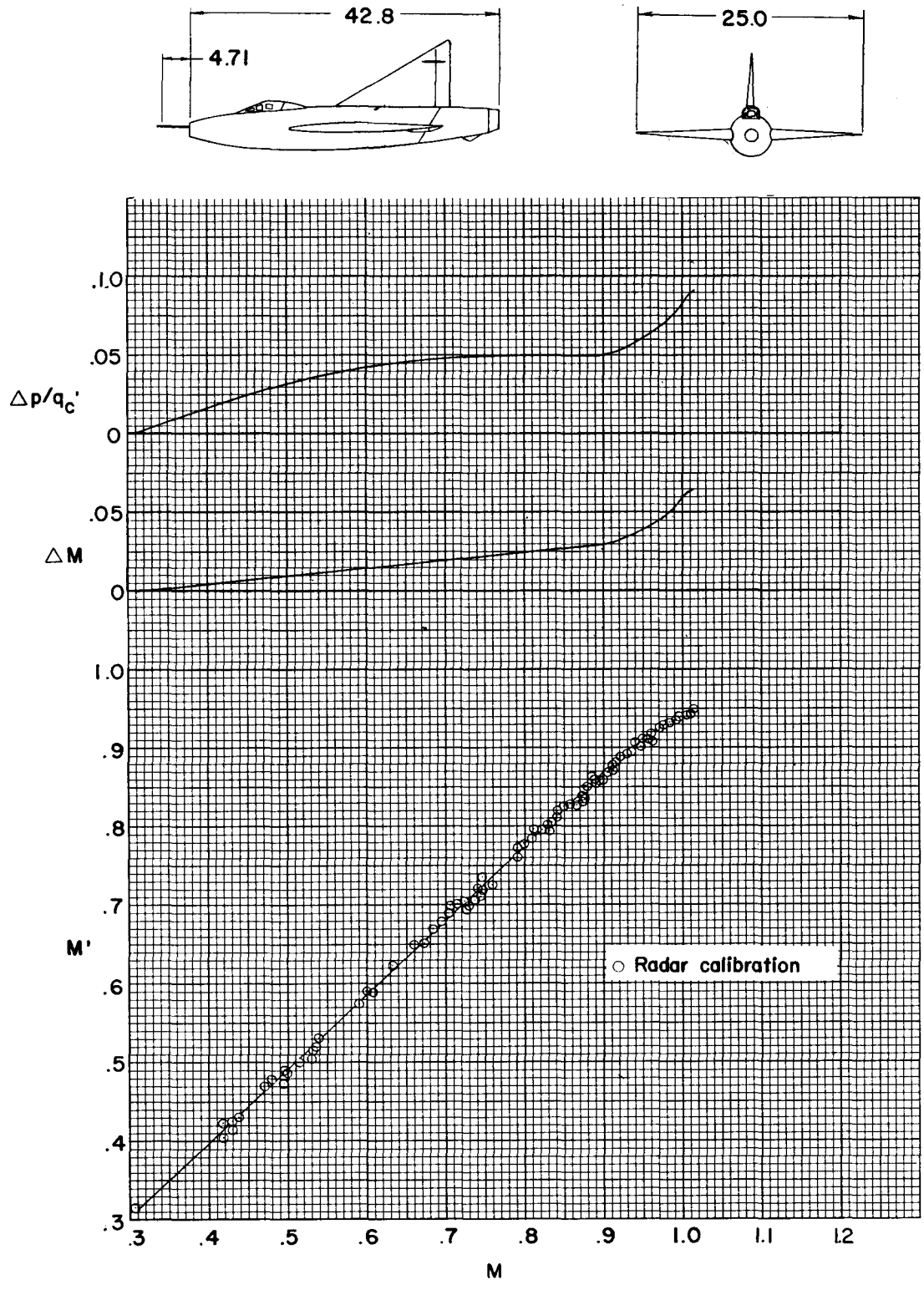

Figure 8.- Static-pressure errors for airplane F.

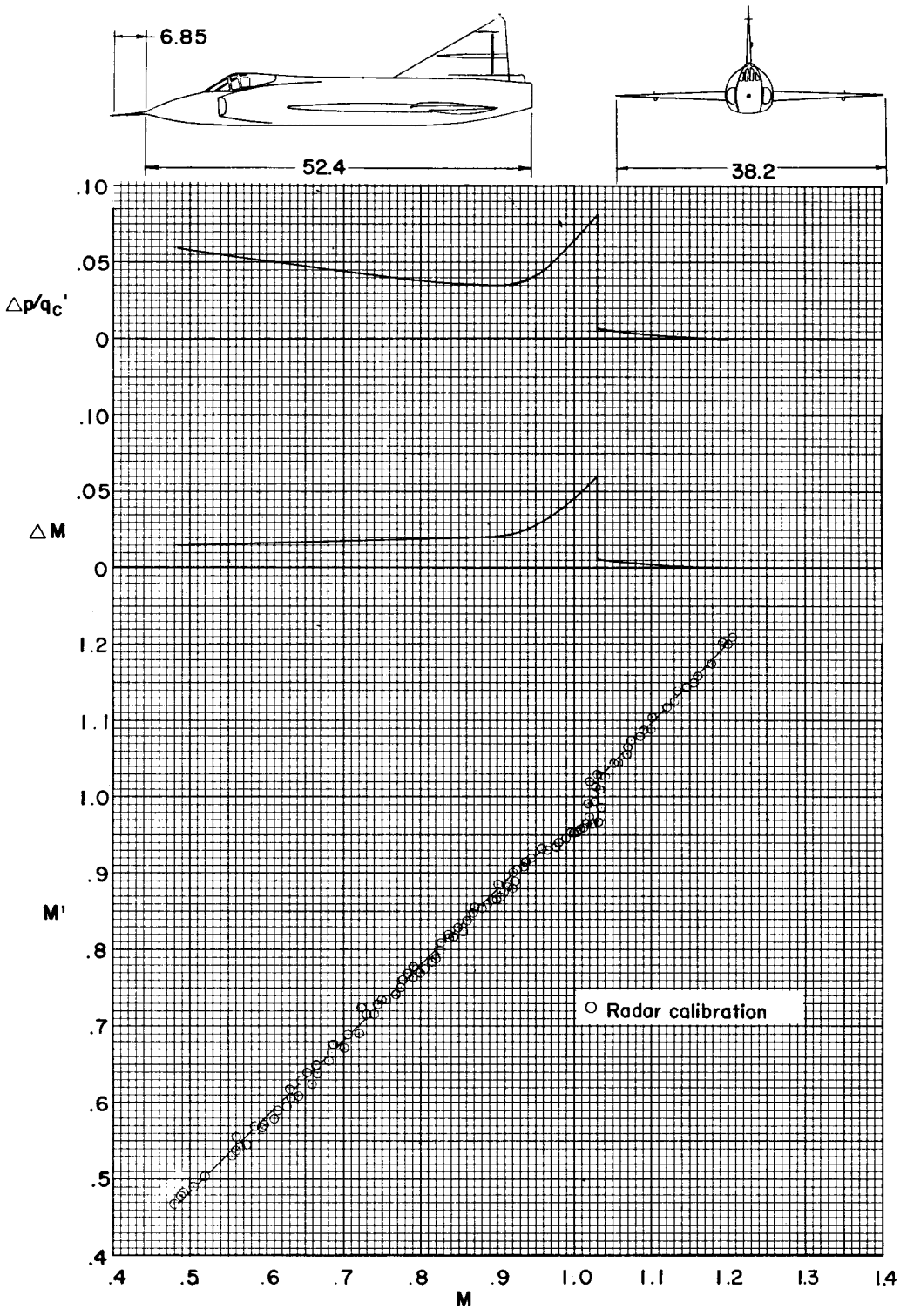

Figure 9.- Static-pressure errors for airplane G.

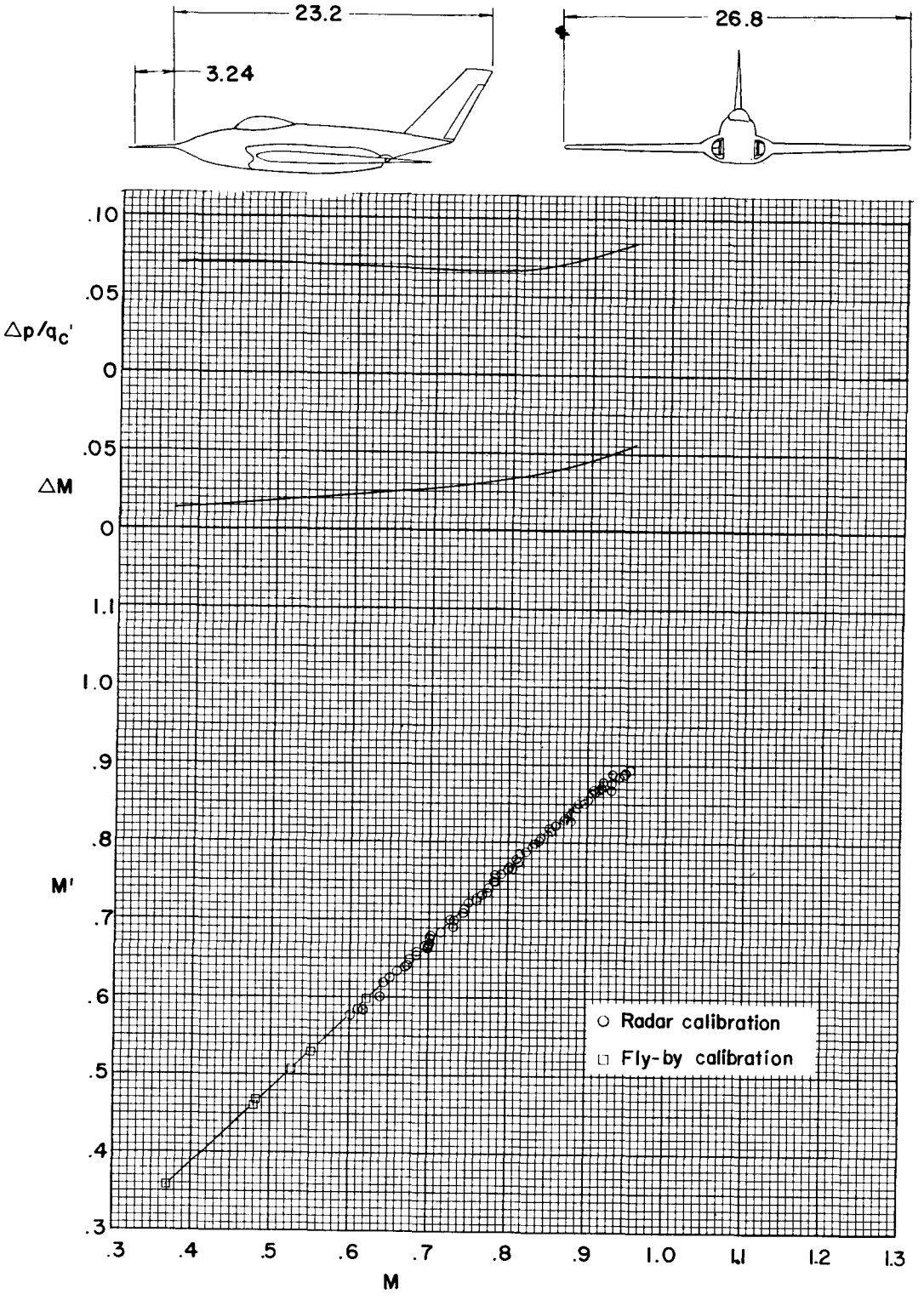

Figure 10.- Static-pressure errors for airplane H.

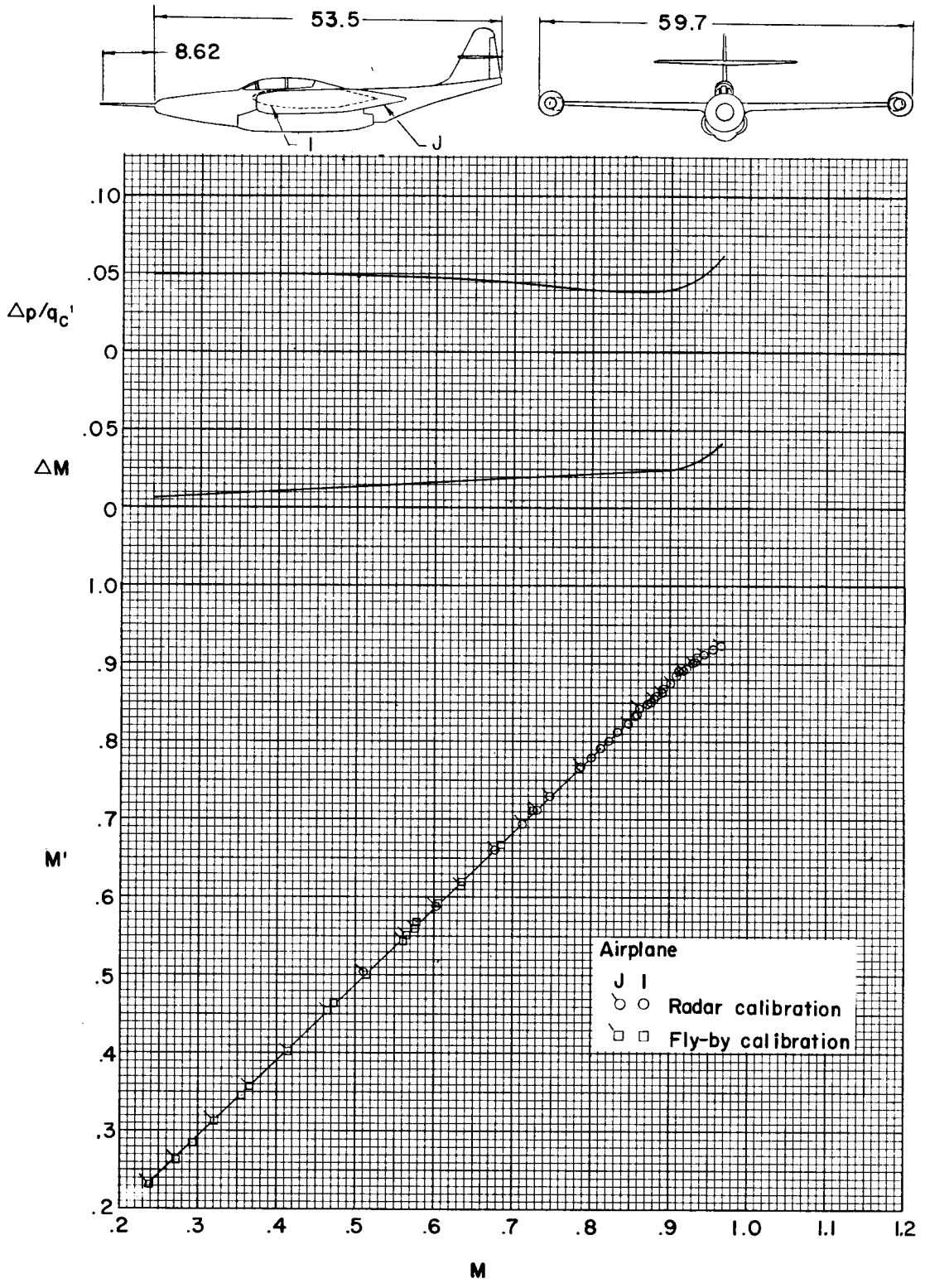

Figure 11.- Static-pressure errors for airplanes I and J.

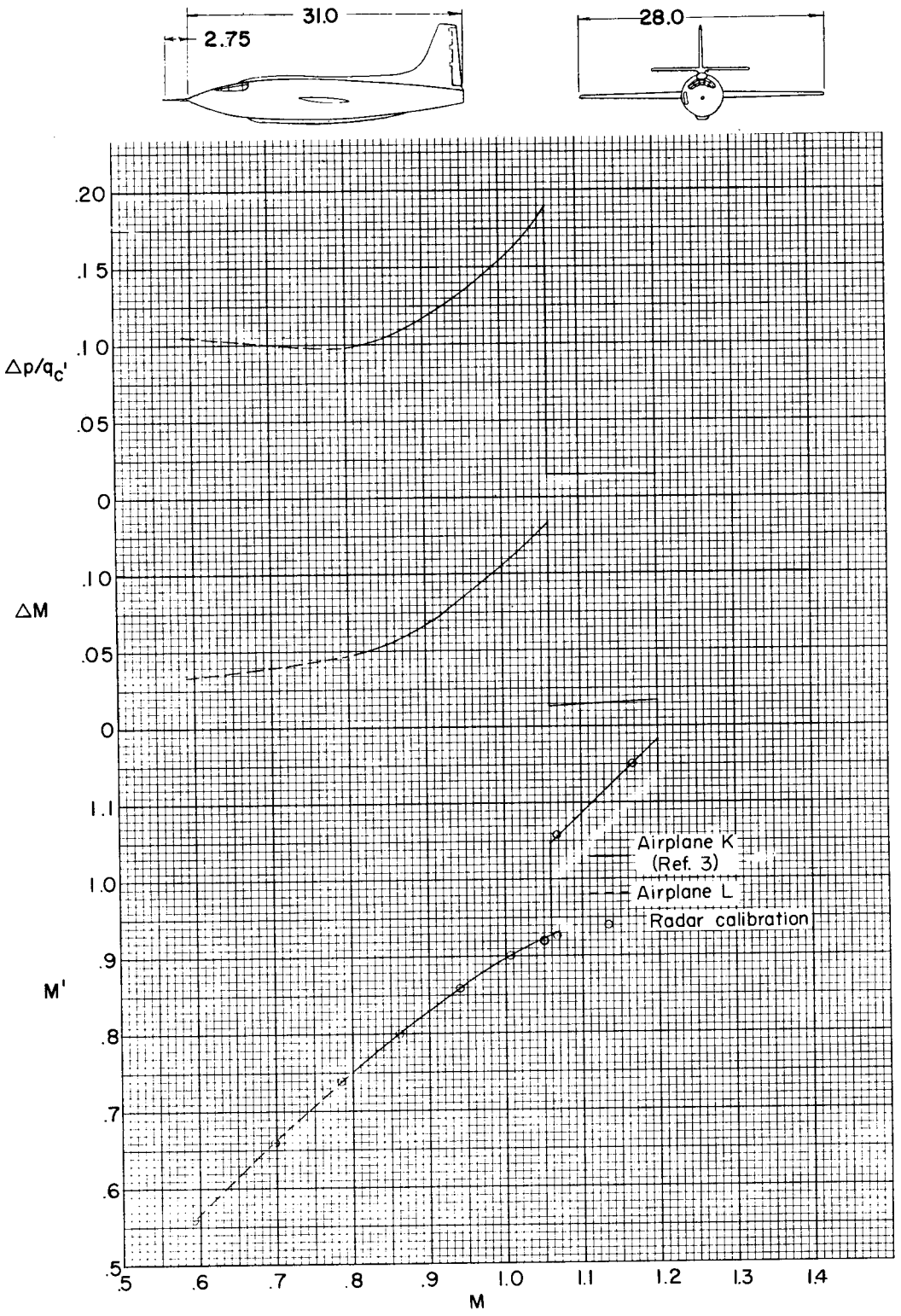

Figure 12.- Static-pressure errors for airplanes K and L.

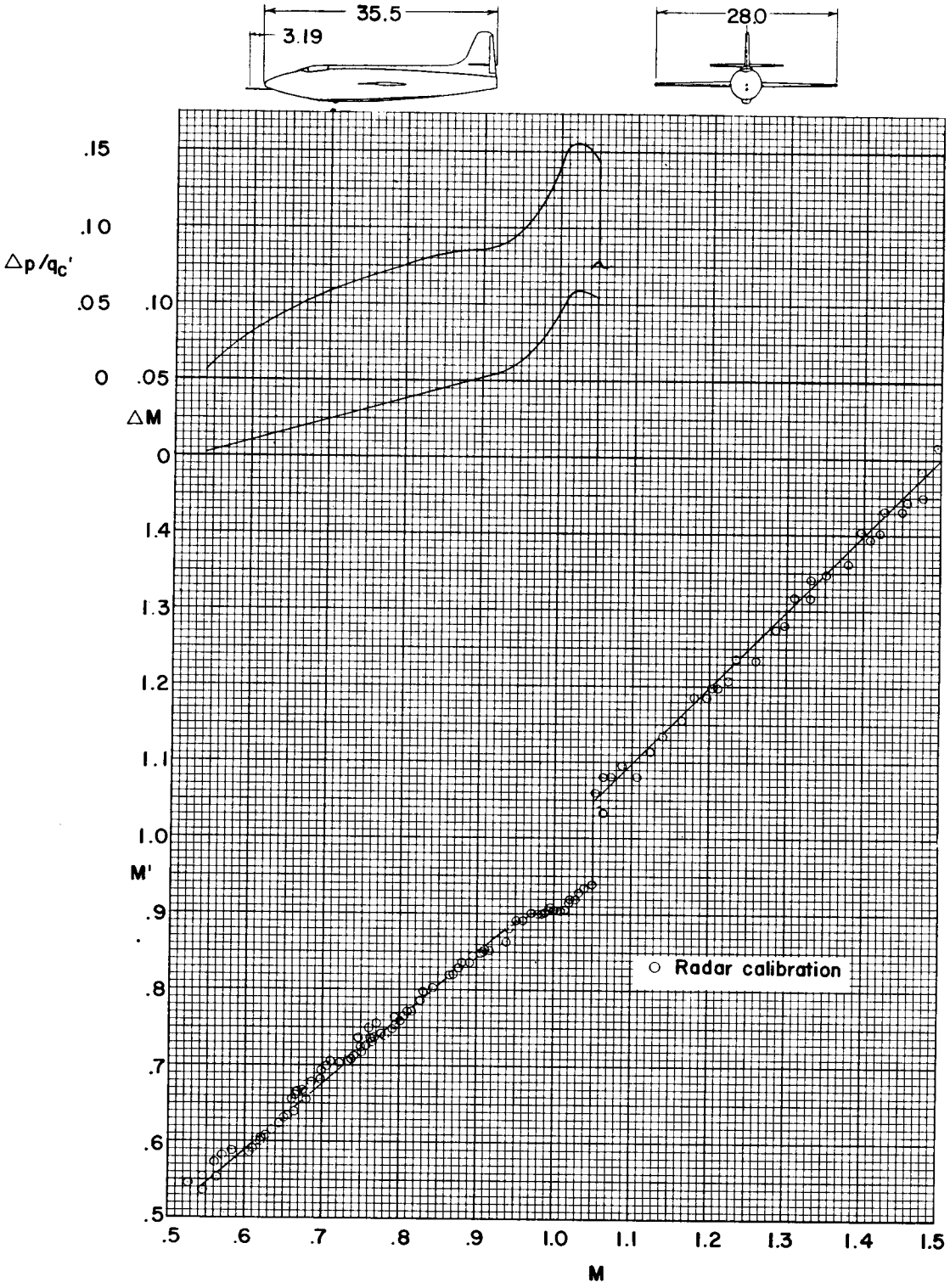

Figure 13.- Static-pressure errors for airplane M.

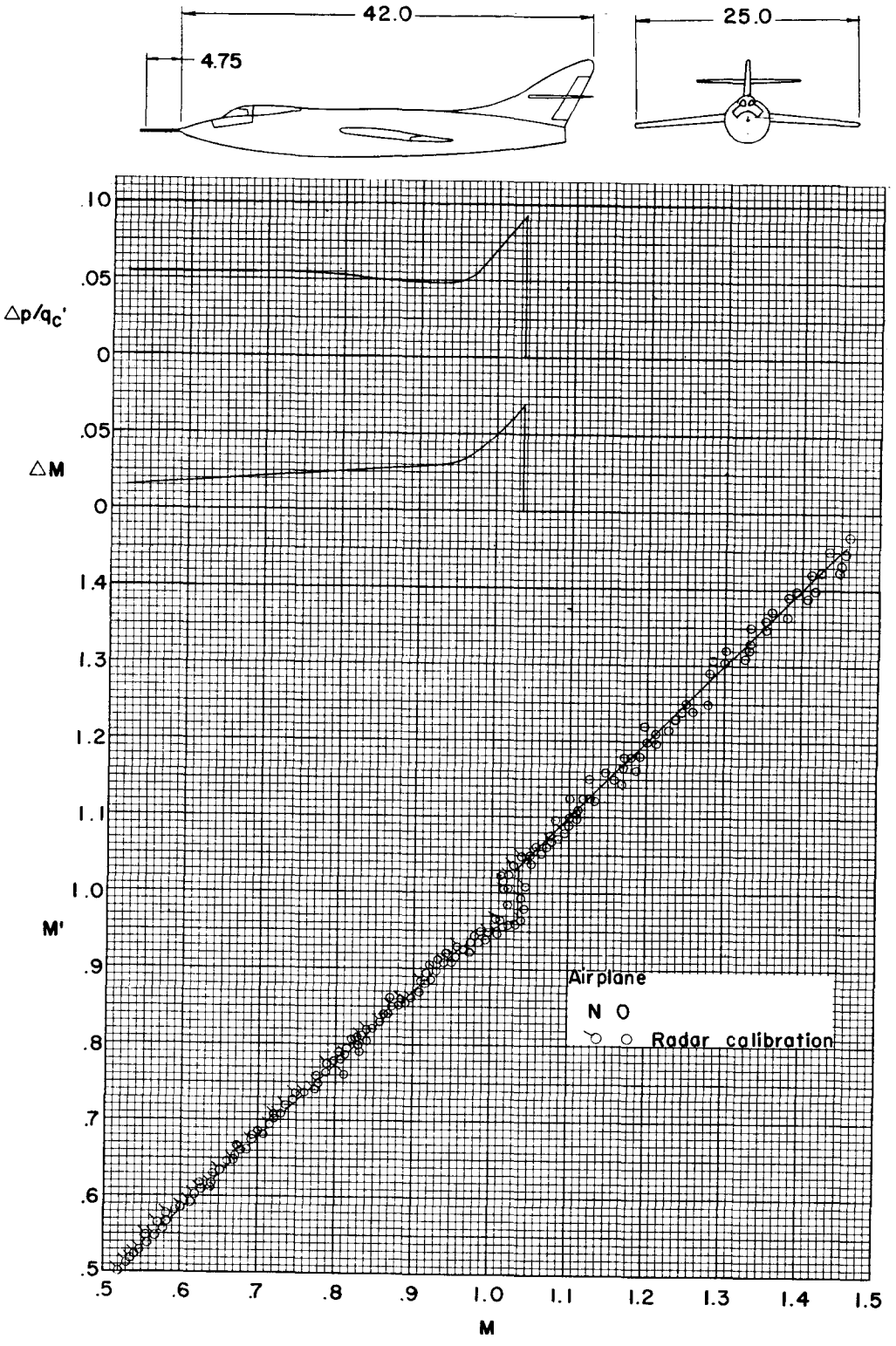

Figure 14.- Static-pressure errors for airplanes N and O.

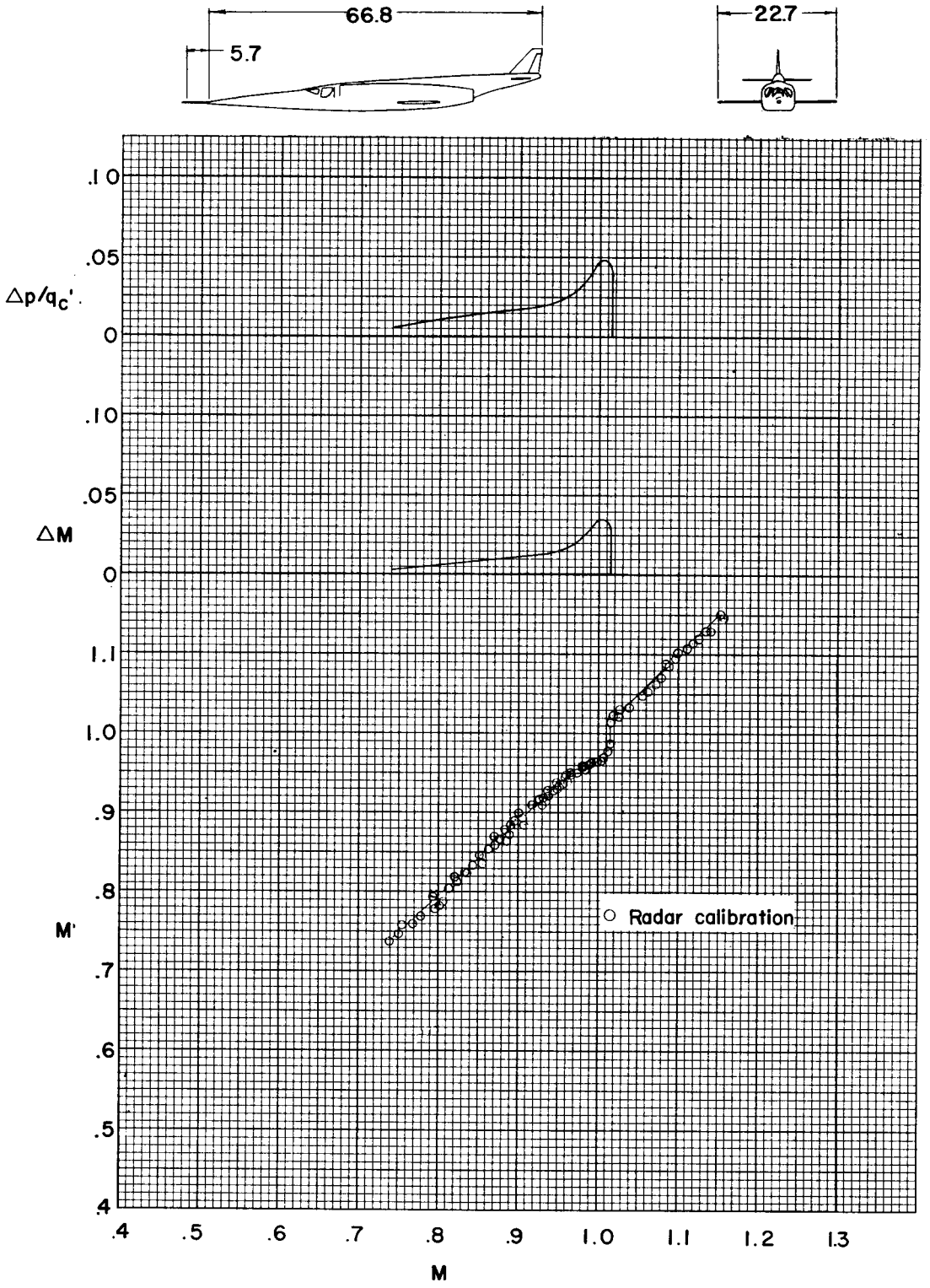

Figure 15.- Static-pressure errors for airplane P.

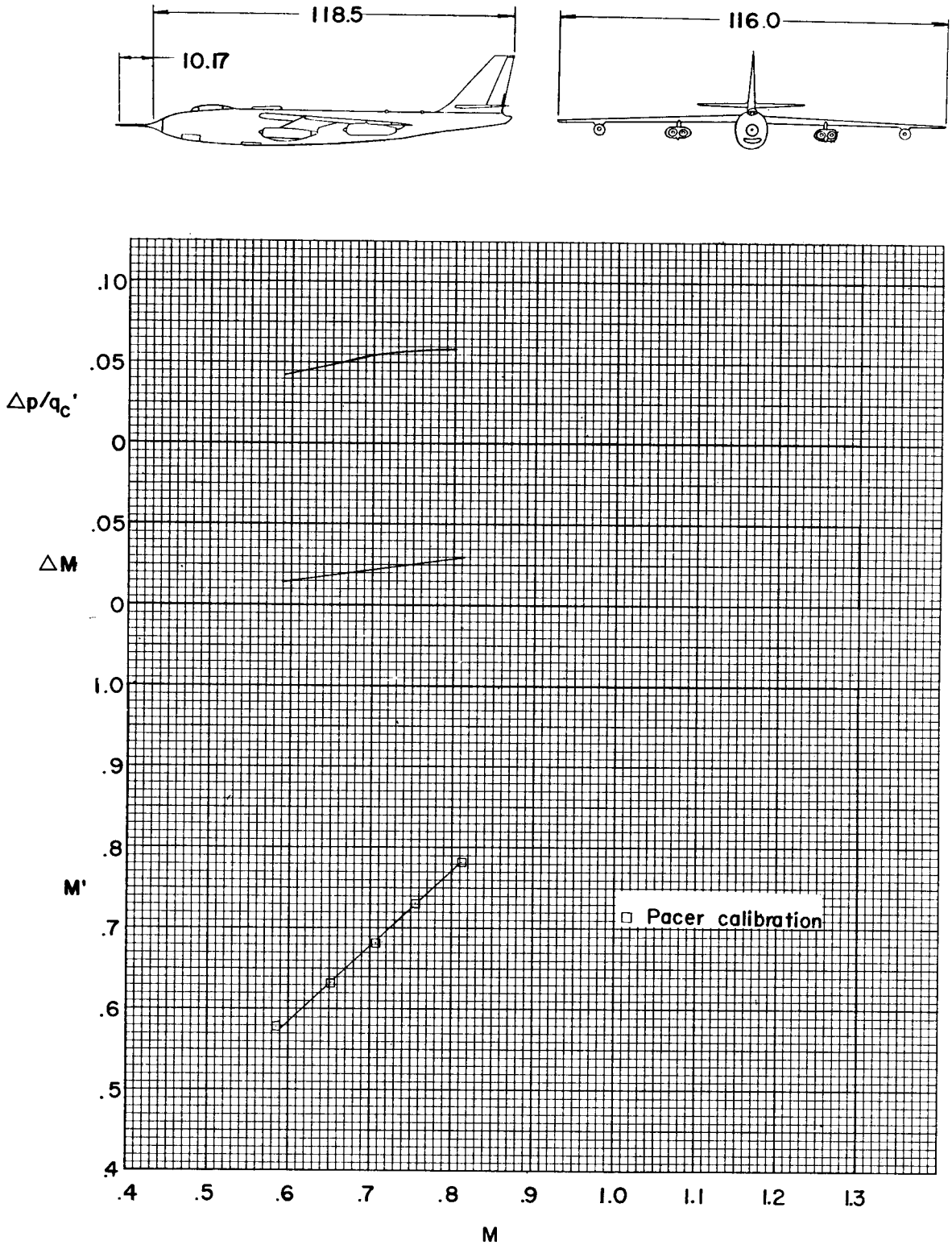

Figure 16.- Static-pressure errors for airplane Q.

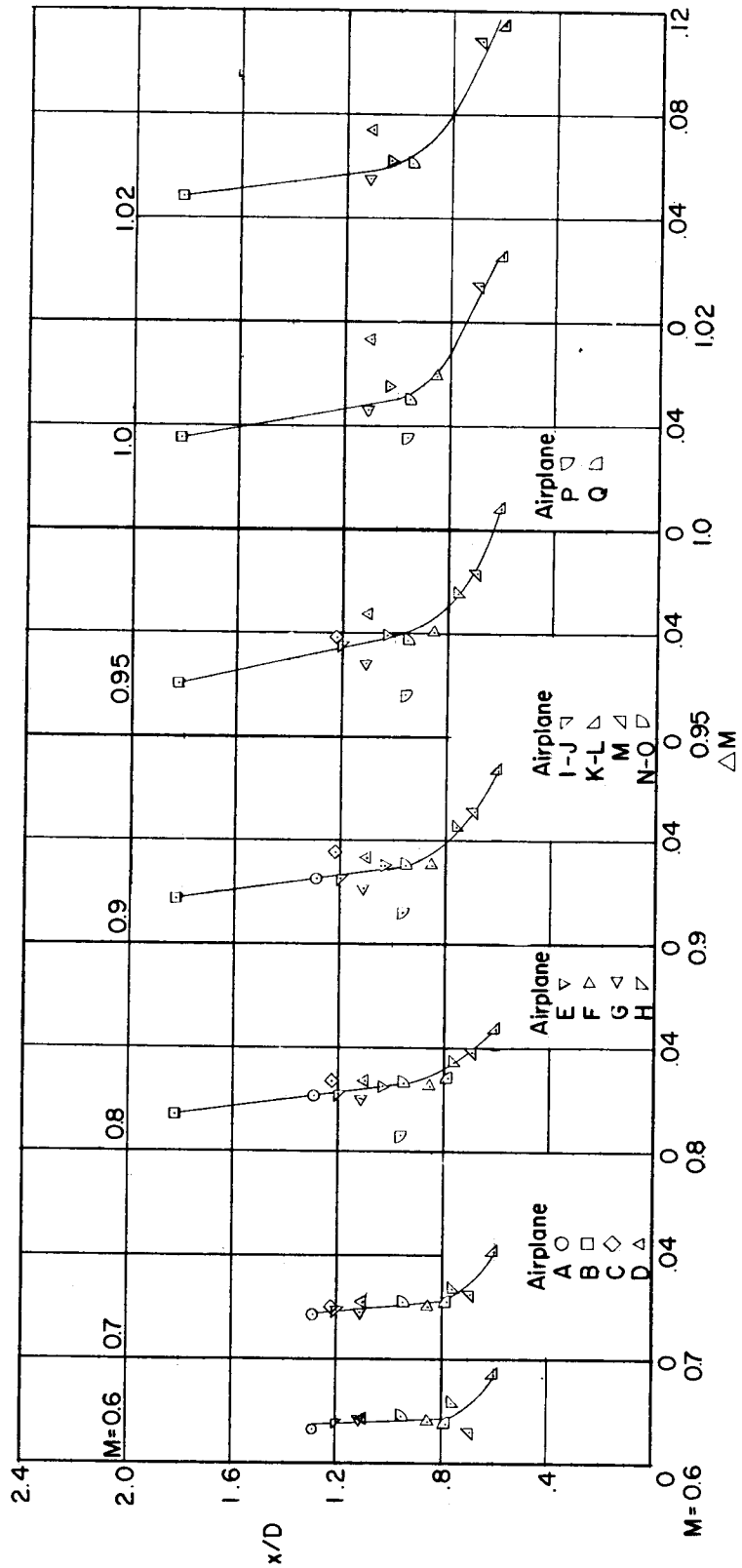

Figure 17.- Variation of Mach number errors with the ratio x/D for the test airplane.

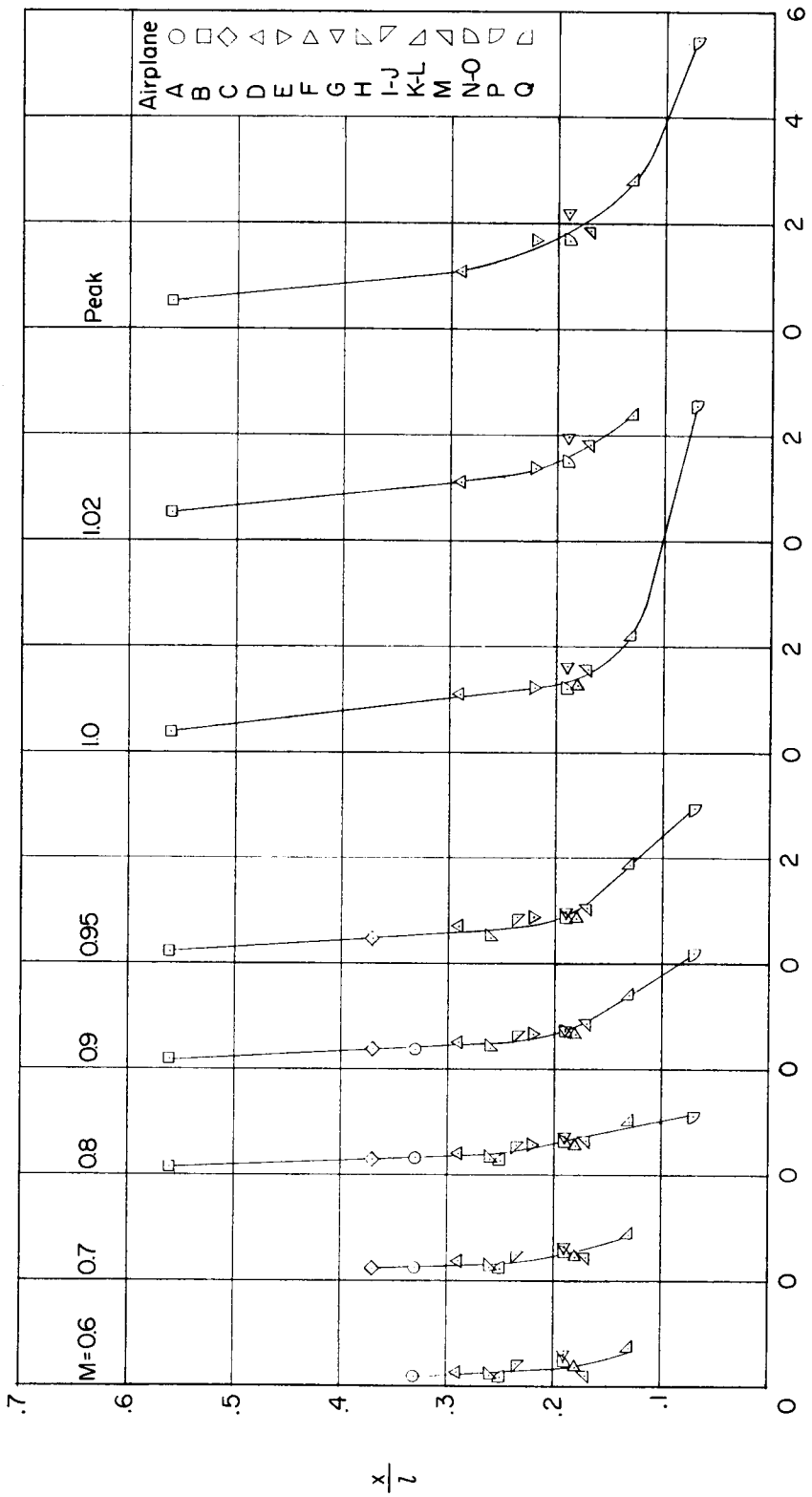

Figure 18.- Variation of $(l/D)^2 \Delta M$ with the ratio x/l for all the test airplanes.

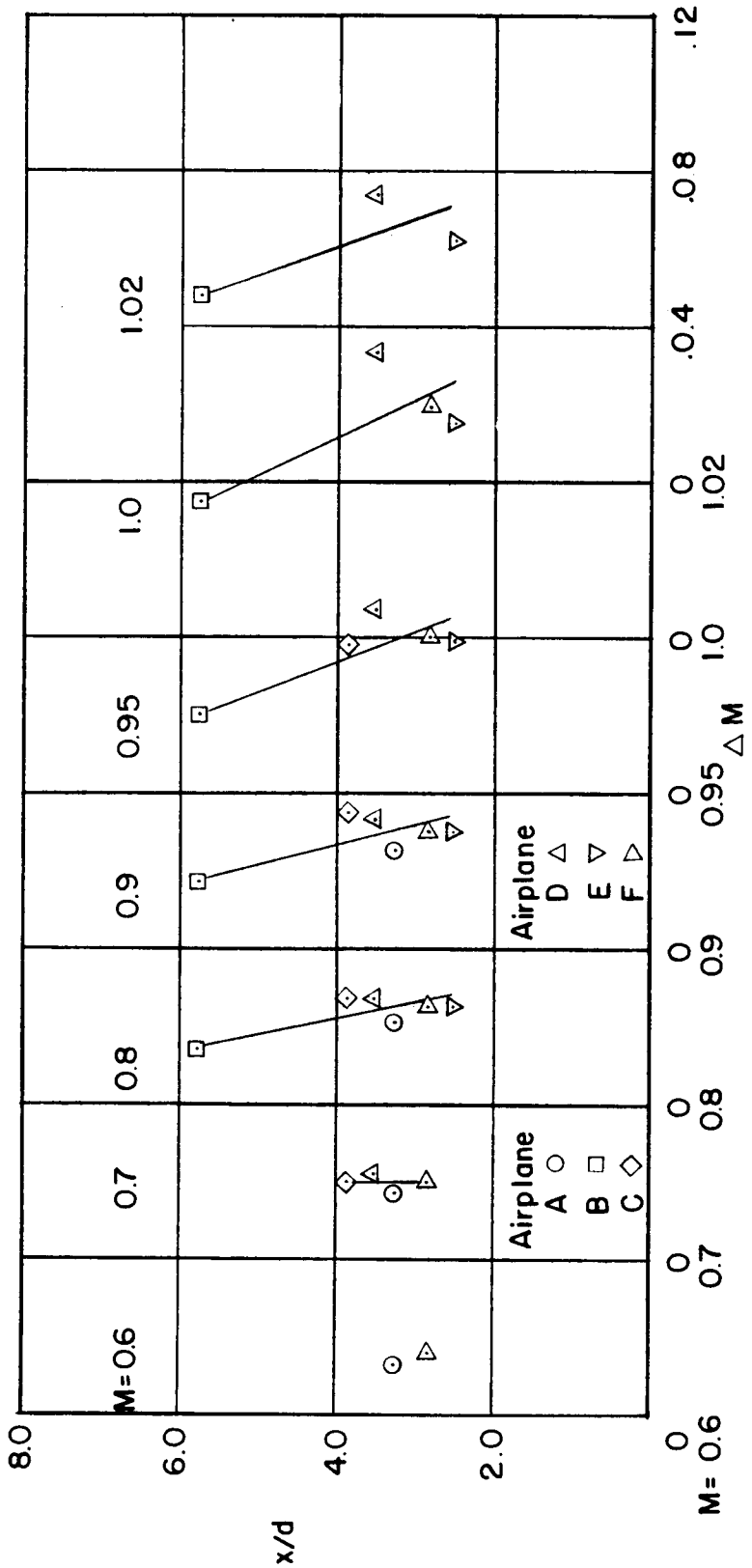

Figure 19.- Variation of Mach number errors with the ratio x/d.